THESIS SUMMARY

A relative moment tensor inversion technique applied to seismicity induced by mining

Lindsay Marguerite Andersen

Abstract

Studies of source mechanisms of mining-induced seismic events play an important role in understanding the various modes of failure observed around underground excavations. These planes of failure can be mapped using conventional techniques, for example, geological fracture mapping. However, such an approach is often problematical due to limited access to the site, poor exposures (if any) of the failure plane, not to mention that fracture mapping is time consuming and requires a degree of experience. An added difficulty is that planes of failure often do not follow faults of geological origin, but are related to the geometry of the advancing stope face. For example, the development of face-parallel shear zones ahead of deep-level stope faces. In such cases, the stresses induced by mining dominate over the geological structure in the critical region close to the stope face. Seismic methods therefore have the potential of being the only practical method of studying the development of seismic shear zones underground.

Slip on such a failure plane generates a three dimensional elastic wave that propagates through the rockmass, carrying a wealth of information regarding the source rupture process. Through a process known as moment tensor inversion, recordings of the ground displacements (measured by seismometers) can be used to calculate a quantity known as a seismic moment tensor. The moment tensor describes the source mechanism of seismic events and gives insight into the mode of failure and geometry of the failure plane.

However, moment tensor solutions computed using conventional methods are sensitive to noise and may be biased due to systematic errors in the measurements. The primary objective of this study was to develop a robust moment tensor inversion method to estimate the moment tensors of clusters of seismic events recorded in the underground environment. To achieve this, three 'hybrid' methods were developed by the author. These methods were iterative and exploit the strengths of both the absolute and relative moment tensor inversion methods. The hybrid methods were essentially weighting schemes designed to enhance the accuracy of the computed moment tensors by decreasing the effect of noisy data and correcting for geophone site effects.

In the hybrid methods, the moment tensor components for each event in the cluster were computed using absolute inverse techniques and then corrections (or weightings) to the input data were applied. The weighting or correction applied to a particular observation was derived from the residuals determined when observed data were compared with corresponding theoretical data (for a particular geophone site, sensor orientation and wave phase) and were calculated using a cluster of events rather than a single event. The relative aspect of the hybrid methods was that a common ray-path between each event in the cluster and a particular receiver was assumed.

An important aspect in the development of any new technique is extensive testing of the algorithm. This formed an intermediate objective of this study. The performance of the hybrid moment tensor inversion methods under various extreme situations was assessed using synthetic data.

The final objective was to determine whether the techniques developed could be successfully applied to real data. The hybrid moment tensor inversion methods using a median and weighted mean correction were applied to a cluster of 10 events, having remarkably similar waveforms, recorded at Oryx Gold Mine. For comparative purposes, the absolute method was also applied. The solutions computed using the hybrid moment tensor inversion using a median correction displayed a distinct improvement after the iterative residual correction procedure was applied. The radiation patterns and fault-plane solutions showed a high degree of similarity, and were probably more accurate reflections of reality than those computed using the absolute moment tensor inversion methods. These observations are very encouraging and point towards the method's potential for use as a standard processing tool for mine seismicity.

The hybrid MTI method is encapsulated in a computer program written by the author called the 'MTI toolbox' and is currently being applied to waveform data recorded in a number of environments: from acoustic emissions recorded in the laboratory, to longer wavelength data recorded on small-scale seismic networks and to large events recorded on mine-wide seismic systems.

The implications of this work are a better understanding of the focal mechanisms of seismic events induced by mining activities, ultimately leading to improved safety underground.

1. Introduction

The seismic moment tensor is a broad concept, which describes the equivalent forces of a general seismic point source. A source can be considered a point source if both the distance of the observer from the source and the wavelength are much greater than the linear source dimension. The seismic radiation pattern and the strength of the seismic point source are completely described by its moment tensor. Analysis of seismic moment tensors is used to distinguish and quantify (estimate) the relative contributions of various source mechanism processes.

Moment tensor inversions have been routinely performed for several years for larger earthquakes recorded at teleseismic distances. However, the application of a moment tensor inversion technique to microseismic events induced by the development of underground excavations is a relatively recent innovation. Only a few works related to the use of moment tensor inversion in source mechanism studies of mining-induced seismic events have been published (e.g. Spottiswoode, 1984; Brawn, 1989), the reason being that the inversion methods are notoriously tedious and prone to errors.

1.1 Factors influencing the accuracy of moment tensors

Moment tensor inversion ('MTI') is one of the best approaches to study the mode of failure of a seismic source, provided that two major assumptions hold. Firstly, it is assumed that the point source approximation is valid (i.e. that the fault plane dimensions are shorter than the wavelength of the seismic waves used in the inversion), and secondly, that the effect of the earth's structure on the seismic waves is modelled correctly. If either of these assumptions does not hold, the resultant moment tensor may contain a large non double-couple component, even if the source mechanism is a double-couple[1] (Streliz, 1978; Barker & Langston, 1982).

A further factor contributing to the presence of 'false' components in the moment tensor is the quality of the available data. The quality of the MTI and reliability of the results depends to a large extent on the number and quality of data points and on the azimuthal coverage of stations around the source. The GIGO principle (Garbage In, Garbage Out) is of particular relevance because data having poor signal-to-noise ratios have an adverse effect on the moment tensor solutions. This last factor forms the main thrust of this study – the development of robust MTI methods to accurately estimate the moment tensor in the underground environment.

The effects of various types of noise on moment tensor solutions are briefly demonstrated to highlight the need for noise reduction techniques. Noisy data has a considerable effect on

[1] A number of theoretical source models have been proposed to explain the P-wave polarity observations. These models consist of various types of forces acting at a point source, rather than on a fault plane, because the former is much simpler to analyse than the latter. The double-couple model, introduced in the 1960s, is the currently accepted model. The double-couple model consists of two pairs of forces. Each pair consists of forces with equal magnitude and opposite directions, so that the total force is equal to zero. In addition, the *torque* of each couple about the origin of the axes is of equal magnitude and opposite to one another so that the total torque is zero.

the MTI and results in the appearance of 'false' components in the solutions. Other unwanted effects are blurring of the radiation pattern and variations in the fault-plane solutions. These effects are briefly demonstrated using both synthetic and recorded data.

Figure 1(a) shows the radiation pattern and fault-plane solutions resulting from the absolute MTI of synthetic data of a pure double-couple source having a strike of 20°, dip of 60° and rake of 0°. (The various inversion types are discussed in the following section.) The fault-plane solutions and three quantities (%ISO, %DC and %DC) describing the source mechanism are calculated from the moment tensor and are listed in the figures. %ISO is the percentage isotropic component, %DC is the percentage double-couple component and %CLVD is the percentage compensated linear vector dipole of the six component moment tensor. The percentage of 'false components' is calculated by adding magnitudes of %ISO and %CLVD because for a pure double-couple source, %DC should be ~100%, and %ISO and %CLVD should both be approximately zero.

It is evident from Figure 1(b) that the percentage of false components is ~8% (this value is not zero because of the less than perfect coverage of the focal sphere that results in a relatively poorly conditioned system of equations). In Figure 1(b), pseudo-random noise at a level of 40% has been applied to the input data. When this solution is compared with that of the noise-free case, the most obvious change is the blurring of the radiation pattern, indicating an increase in non double-couple components. The percentage of false components increases from ~8% to ~22%. In addition, there is a slight decrease in the accuracy of the fault-plane solutions.

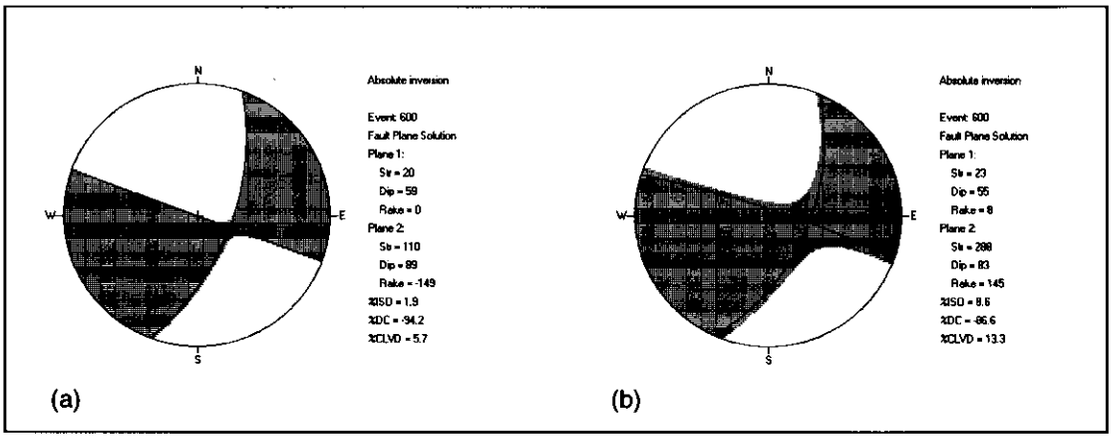

Figure 1: Radiation patterns and source parameters computed from synthetic data using the absolute MTI technique. (a) Noise free case. (b) 40% random noise applied to all channels.

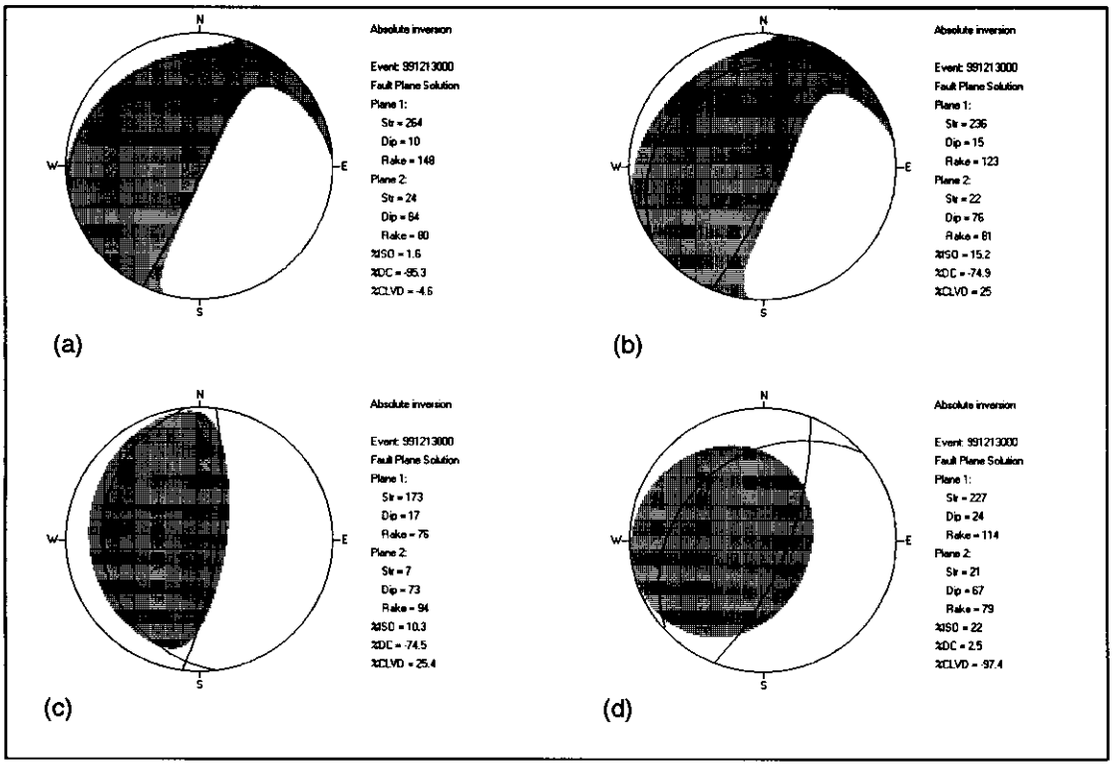

Figure 2: Radiation patterns and source parameters computed from recorded data using the absolute MTI method (a) Control case, (b) 40% random noise applied to all channels, (c) reversed P- and S-wave polarities for site 1, and, (d) bad phase picks for P- and S-wave for site 1, component 1.

In Figure 2, a number of different forms of noise are inflicted on the input of the absolute MTI. The results shown are computed using recorded data. Figure 2(a) shows the radiation pattern, fault-plane solutions and source parameters of the control case i.e. the solution computed from seismograms having accurate P- and S-wave picks where no synthetic noise has been applied. The percentage of false components is ~6%. The radiation pattern of this event becomes slightly blurred when 40% pseudo-random noise is applied to the input data (Figure 2b). In Figure 2(c), the polarities of the waveforms recorded by site 1 have been reversed, and, Figure 2(d) shows the effect that incorrect P-and S-wave picks have on the moment tensor solution (for site 1 and component 1). In all cases, except for the control case, the percentage of false components present in the solution increases as a result of the applied noise. This is accompanied by a blurring of the radiation pattern and change in the fault-plane solution.

1.2 Classification of MTI methods

Numbers of MTI techniques have been proposed since the pioneering paper of Gilbert & Dziewonski (1975). The models of the seismic source and the methods applied differ greatly according to the available data and the purpose of the study. In this thesis, a distinction is made between the 'absolute' and 'relative' methods. These broad classes of inversion procedure are based on methods used to estimate the Green's functions, which describe the wave propagation between the source and receiver.

In the absolute methods, the wave propagation is evaluated theoretically or determined empirically from observations and a known source. One of the difficulties in the absolute inversion (apart from noise affecting the input data) is the accurate estimation of the Green's functions for geologically complex media. In structurally complex environments, with possible lateral inhomogeneities, it is not always possible to calculate the Green's functions with adequate accuracy. The result is the introduction of systematic errors into the moment tensor elements. In the mining situation, it is possible to take measurements using geophones placed at depth, thereby removing the effect of surface weathering. However, this advantage is offset, or possibly exceeded, by the effect of mining voids on the seismic ray-paths.

In contrast to the absolute methods, the relative inversion methods do not require the calculation of theoretical Green's functions for each event. Relative methods are based on the concept of a common ray-path between a cluster of seismic sources and any receiver, and assume that all the events in the cluster experience the same wave propagation effects to each receiver. Generally, the radiation pattern of a reference event is used to estimate the Green's functions for events from the same source region (e.g. Patton, 1980; Strelitz, 1980; Oncescu, 1986). In the relative method proposed by Dahm (1996) (known as the relative method without a reference mechanism) the path effects described by the Green's functions are eliminated analytically – thereby completely avoiding the explicit use of the Green's functions. However, this method is applicable to clusters of events having different radiation patterns only and, because there is no absolute reference, any of the six components of the moment tensors can be incorrect by an unknown scaling factor. This syndrome can be reduced, but not eliminated, through reference to scalar moment estimates. Furthermore, when the mechanisms are similar the method is extremely sensitive to noise. This is a serious disadvantage in the underground environment where clusters of recorded events might have very similar mechanisms. This problem is accentuated when the method is applied to very small events having similar mechanisms and with signals just above the noise level.

2. Hybrid MTI

A problem common to the absolute and relative MTI methods is their sensitivity to noise or errors in the observations and their dependency on accurate Green's functions to describe the wave propagation. Factors such as the focusing and defocusing of the ray-paths in structurally complex environments, the degradation of the velocity model due to mining-induced fractures and mining voids on the seismic ray-paths, low signal-to-noise ratios and poor P- and S-wave picks all have adverse effects on the accuracy of the MTI.

The deviations in the ray-paths between a cluster of seismic sources and a particular recording site can result in consistently high or low amplitudes for all the events recorded at that site, resulting in the introduction of systematic errors into the moment tensor elements. The hybrid methods developed by the author were designed to compensate for the various forms of systematic error. In addition to compensating for the various types of systematic error influencing the waveforms recorded in the underground environment, the hybrid methods can also be used to enhance signals recorded near a nodal plane in the radiation pattern or to decrease the influence of a low quality observation.

The hybrid methods are in essence weighting schemes that aim to increase the accuracy of the computed moment tensor by diminishing the effect of noisy data on the system of equations and correct for site effects. Various weighting schemes have been proposed in the literature (Udias & Baumann, 1969, Šílený *et al.*, 1992). The schemes investigated were applied to individual events and the corrections (or weightings) were determined using the residuals computed for the event of interest. The new aspect of the hybrid methods proposed herein is that the correction applied to a particular observation is based on the residuals (for a particular geophone site, channel and phase) calculated using all of the events in the cluster – this constitutes the relative component of the hybrid methods. The weighting schemes are non-linear and are applied iteratively.

An analogous approach has been applied to the seismic location problem, *viz.* the so-called 'JHD method' (joint hypocentral determination). The relative locations obtained through JHD are usually better than those determined by inversion of more complete and complex velocity models, and the resulting hypocentral locations often give a more focussed picture of the seismicity.

2.1 Conceptual outline of hybrid MTI methods

Statistical theory shows that the distributions of the errors of measurement are remarkably regular, i.e. the distributions can be closely approximated by continuous curves referred to as normal error curves. Using this knowledge, the effect of outliers (data points whose residuals lie 'far' from the mean or median error) can be downgraded by the application of the relevant weighting. The errors or residuals indicate the extent of 'misfit' of the solution with the measured data, and are the result of a number of error sources. Such sources would include the errors originating from incorrect picks and/or poor identification of the various wave phases, low signal-to-noise ratios, deviations in the ray-paths, and amplification or damping of the signal due to local site conditions, etc.

The concept of a weighting scheme is not a new one, and various schemes have been described in the literature. The method proposed by Udias & Baumann (1969) is perhaps the most relevant to this work. Their weighting scheme is based on the standard deviation of the residuals of the polarisation angles of the S-wave, and on the number of stations with inconsistent P-wave data. These two values are combined into a total error whose minimum is sought. The weighting scheme developed by these workers is based on the distribution of errors for individual events. In contrast to Udias & Baumann (1969), the weighting schemes proposed in this thesis are based on the residuals computed when measured data are compared with theoretical data (for a particular geophone site, channel and phase) and are calculated (for a particular geophone site, channel and phase) using all of the events in a cluster, rather than an individual event.

The weighting factors are computed in three different ways. In Scheme A, the weights are related to the mean of the distribution of residuals. This approach is probably the least robust of all the proposed schemes, since a single large outlying value can dominate the mean (and often does so, owing to the relatively small number of observations or 'data points'). Because of the problems associated with outliers, Scheme A is merely of academic interest but is included for comparative purposes and to emphasise the need for the schemes that follow. In Scheme B, the weights are related to the median of the distribution of residuals, so that the effect of a solitary outlier is diminished. In Scheme C, a weighting

scheme is used which is based on a data point's distance (measured in standard deviations) from the mean error.

Once the weightings have been applied to the observations, a new set of moment tensor components is computed using the absolute technique. From the new set of moment tensors, a new set of weights is computed. The weights are then applied to the corrected observations, which are subsequently used as input to the absolute MTI as before. (In addition to the weights determined from the residuals, Schemes A and B incorporate a second weighting factor to control the proportion of the weights applied with every iteration.) The process is applied iteratively until a predefined criterion or set of criteria is satisfied. Schemes A, B and C are illustrated conceptually in Figure 3.

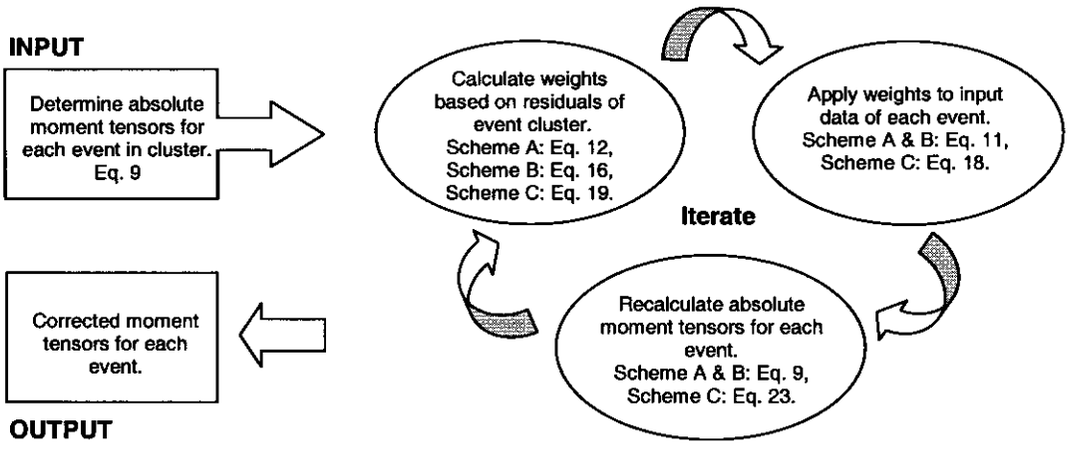

Figure 3: Conceptual flowchart illustrating the hybrid MTI methods.

2.2 Theoretical description of hybrid MTI methods

The goal of all MTI methods is to use observed values of ground displacement to infer properties of the source, as characterised by the moment tensor. By using the representation theorem for seismic sources (Aki & Richards, 1980) and assuming a point source, the displacement field u_k recorded at a receiver k is given by:

$$u_k(x,t) = G_{ki,j}(x,t;\xi,t') * M_{ij}(\xi,t') \qquad [1]$$

where $G_{ki}(x,t;\xi,t')$ are the elastodynamic Green's functions containing the propagation effects between the source (ξ,t') and receiver. The comma between the indices in Equation [1] describes the partial derivatives at the source with respect to the coordinates after the comma, i.e. $G_{ki,j} = \frac{\partial G_{ki}}{\partial \xi_j}$. The $M_{ij}(\xi,t)$ terms are the nine time-dependent components of the moment tensor.

As the equivalent body forces conserve angular momentum, $M_{ij} = M_{ji}$, only six of the components are required. Equation [1] can be simplified further, by assuming that all of the moment tensor components have the same time-dependency (synchronous source approximation). The temporal part of the moment tensor can then be separated such that

$$M_{ij}(t') = M_{ij}s(t') \qquad [2]$$

where M_{ij} is a set of constant terms, and $s(t')$ is referred to as the source-time function. Equation [1] becomes:

$$u_k(x,t) = \left[G_{ki,j}(x,t;\xi,t') * s(t')\right]M_{ij} \qquad [3]$$

It can be further assumed that the equivalent forces act very simply in time i.e. that the source-time function is an impulse: $s(t) = \delta(t)$. Then the convolution of $G_{ki,j}$ with $\delta(t)$ will be equal to itself i.e. $G_{ki,j}(x,t;\xi,t') * s(t') = G_{ki,j}$. Equation [3] then simplifies to a linear equation:

$$u_k = G_{ki,j}M_{ij} \qquad [4]$$

Equation [4] can be written in matrix notation as:

$$\mathbf{u} = \mathbf{G}\,\mathbf{m} \qquad [5]$$

where the vector **u** consists of sampled values of the integrated ground displacement or spectral plateaus depending on whether a time or a frequency-domain approach is being taken and is a vector of dimension n. The matrix **G** is composed of the Green's functions in the coordinate system of the receivers and has dimensions $n \times 6$. **m** is a vector consisting of the moment tensor components $M_{11}, M_{22}, M_{33}, M_{12}, M_{13}$ and M_{23}. Each component of each station is stacked into the **u** vector while the appropriate Green's function is put into the **G** matrix. In most cases $n >> 6$ and the system of equations is, in principle, overdetermined. In order to solve for the components of the moment tensor **m**, Equation [5] is written as an inverse problem such that:

$$\mathbf{m} = \mathbf{G}^{-1}\mathbf{u} \qquad [6]$$

where $\mathbf{G}^{-1}$ is the generalised inverse of **G**.

In the weighting schemes that follow, corrections are made to the input data. The corrections are made in stages to maintain stability and to track changes in the moment tensor solutions. Each of the weighting schemes are based on the absolute inversion method described by Equation 1 to 6. However, it is important to note that in this section the notation is extended slightly, to indicate that the equations are applied to an event (the i^{th} event) in a cluster (of N events), rather than to a solitary event. Accordingly, Equation 5 is rewritten as:

$$\mathbf{u}_i^{obs} = \mathbf{G}_i\,\mathbf{m}_i \qquad [7]$$

where the subscript i indicates that Equation 7 applies to the i^{th} event in a cluster and the superscript *obs* indicates that the data contained in the $\mathbf{u}_i$ vector are observed values (to distinguish between theoretical values computed later in this section) .

Vectors and matrices are denoted using **bold** letters, and elements of vectors and matrices are given using the same letter but in *italics*. For example, $\mathbf{u}_i^{obs}$ is a vector of observed amplitude data for event i containing M elements of the form u_{ijkl} where: the first subscript i indicates the event number and $i = (1, 2, 3, \ldots, N)$ where N is the maximum number of events in the cluster; the second subscript j denotes the site number where $j = (1, 2, 3, \ldots, P)$ and P is the maximum number of geophone or observation sites; the third subscript k describes the component of the three component sensor and $k = (1, 2, 3)$; the fourth subscript l indicates the indicates wave phase such $l = 1$ for the P-phase and $l = 2$ for the S-phase.

Applying these conventions and considering each equation of the system of equations given by Equation 7, the displacement of the i^{th} event recorded at the j^{th} site for geophone component k and phase observation l is related to the components of the Green's functions and moment tensor components by:

$$u_{ijkl}^{obs} = \sum_{r=1}^{6} G_{ijklr} m_{ir} \qquad [8]$$

Scheme A - mean correction

1. Consider a cluster of N events. The components of the moment tensor $\mathbf{m}_i$ of the i^{th} event in the cluster can be computed by writing Equation 7 as an inverse problem and solving for the vector $\mathbf{m}_i$ such that:

$$\mathbf{m}_i = \mathbf{G}_i^{-1} \mathbf{u}_i^{obs} \qquad [9]$$

   where $\mathbf{G}_i^{-1}$ is a $6 \times M$ matrix and is the generalised inverse of $\mathbf{G}_i$. Since M > 6 the system of equations is overdetermined and Equation 9 is solved using the method of least-squares. This approach fits the set of known amplitude data of event i, $\mathbf{u}_i^{obs}$, to a Green's function matrix, $\mathbf{G}_i$, by computing the most statistically suitable moment tensor $\mathbf{m}_i$ for that event.

2. Once the moment tensors $\mathbf{m}_i$ are computed for each event i in the cluster, the theoretical displacements are $\mathbf{u}_i^{th}$ computed using the forward calculation:

$$\mathbf{u}_i^{th} = \mathbf{G}_i \mathbf{m}_i \qquad [10]$$

In general, $\mathbf{u}_i^{th} \neq \mathbf{u}_i^{obs}$ because the system is overdetermined, and the $\mathbf{m}_i$ are the results of the least-squares fit. This fact plays a critical role in the process of hybrid inversion because if $\mathbf{u}_i^{th} = \mathbf{u}_i^{obs}$ the weighting scheme would have no effect (since the correction would equal zero).

3. A correction or weighting determined by consideration of all the events in the cluster is applied to the input displacements such that:

$$u_{ijkl}^{new} = u_{ijkl}^{old} + \underbrace{a_{jkl} \cdot u_{ijkl}^{old}}_{\text{Correction factor}} \qquad [11]$$

where a_{jkl} is a compound weighting function and $u_{ijkl}^{old} = u_{ijkl}^{obs}$ for the first iteration only since u_{ijkl}^{old} will be different for each iteration as a result of the correction applied in Equation 11.

The compound weighting function a_{jkl} is defined according to:

$$a_{jkl} = w_{IterNo} \cdot \left(\bar{r}_{jkl} - 1\right) \qquad [12]$$

In Equation 12, w_{IterNo} is an attenuation function that ranges between 0 and 1 and controls the amplitude of the applied correction or weighting. The term in brackets $\left(\bar{r}_{jkl} - 1\right)$ is a smoothing function determined from the mean ratio $\bar{r}_{jkl}$ between the theoretical $\mathbf{u}_i^{th}$ and observed $\mathbf{u}_i^{obs}$ displacements for the j^{th} site, k^{th} component and l^{th} phase and is computed according to:

$$\bar{r}_{jkl} = \frac{1}{N_{eq}} \sum_{i=1}^{N_{eq}} \left(\frac{u_{ijkl}^{th}}{u_{ijkl}^{obs}} \right) \qquad [13]$$

where N_{eq} is the number of equations and is less than or equal to the number of events N in the cluster. N_{eq} would be less than the total number of events in the cluster if one or more of the geophones were inactive during the occurrence of an event, as is often the case in a mine seismic network. Since the mean ratio $\bar{r}_{jkl}$ is computed using all the events in the cluster (for i = 1 to N_{eq}) for each site (subscript j), component (subscript k) and phase (subscript l) the $\left(\bar{r}_{jkl} - 1\right)$ term may be thought of as a 'site correction'.

The motivation for using w_{IterNo} is to introduce the correction or weighting gradually in order to gauge the smoothness (or otherwise) of the method's convergence. The selection of w_{IterNo} is subjective and a number of other functions could be used. In this study, w_{IterNo} is calculated using:

$$w_{IterNo} = \frac{10^{(IterNo-1)/10}}{10} \qquad [14]$$

i.e. $w_{IterNo} = \{0.10, 0.12, 0.15, 0.19, 0.25, 0.32, 0.40, 0.50, 0.63, 0.79, 1.0\}$. It is evident from the formulation that the maximum number of iterations is 11 and that the weight of the applied correction increases slowly at the beginning of the iterative procedure, and accelerates during the final stages.

The $(\bar{r}_{jkl} - 1)$ term of Equation 12 behaves like a smoothing function. When $u_{ijkl}^{th} = u_{ijkl}^{obs}$ for all events in the cluster (i.e. for i = 1 to N_{eq}), $\bar{r}_{jkl}$ would equal 1, and as a result, $a_{jkl} = 0$. In other words, when the theoretical and observed values of displacement are equal, no correction would be applied. This is hardly ever the case for recorded data and would only occur using synthetic data.

When $u_{ijkl}^{th} \approx u_{ijkl}^{obs}$ for most of the events in the cluster, $\bar{r}_{jkl} \approx 1$ resulting in a_{jkl} being a small value close to zero. In this case, since the observed and theoretical displacements are so similar, the observed data can be considered to have a high degree of accuracy. A very small correction would be applied to the relatively more accurate observed data.

If $u_{ijkl}^{th} > u_{ijkl}^{obs}$ for most of the observed and theoretical displacements, then $\bar{r}_{jkl} > 1$ (Equation 13). As a result, a_{jkl} will be positive and the correction will be added to the observation. This assumes $u_{ijkl}^{th} > u_{ijkl}^{obs}$ implies that the observations at the geophones are being underestimated (due to site effects, noise, etc.) and therefore require amplification.

The reverse is true if $u_{ijkl}^{th} < u_{ijkl}^{obs}$ for most of the equations. In this case, $\bar{r}_{jkl} < 1$ and a_{jkl} will be negative. Consequently, the correction will be subtracted from the observation. It is assumed that $u_{ijkl}^{th} < u_{ijkl}^{obs}$ implies that the observations are being overestimated and therefore require damping.

4. A new set of moment tensors is then recomputed for each event using the corrected data:

$$\mathbf{m}_i^{new} = \mathbf{G}_i^{-1}\mathbf{u}_i^{new} \qquad [15]$$

Return to step 2 and recompute the theoretical displacements using Equation 10, from which a revised correction can be computed as in steps 3 and 4. Iterating through this sequence, the 'best' solution is identified on the basis of the minimum standard error normalised against the scalar moment. The normalisation procedure introduced allows comparisons of the standard errors between iterations. It is necessary because the amplitudes of the linear equations are affected by the weighting scheme, causing changes in the magnitude of the standard error.

Since the *mean* error ratio contributes to the site correction, this scheme is very sensitive to outliers (outliers are defined as the minimum or maximum values of the ratio described by Equation 13). Outliers with large magnitudes will tend to swamp the correction, biasing it towards the less accurate data. For this reason, a Scheme B is developed, where the site correction is based on the median.

Scheme B – median correction

This scheme is almost identical to Scheme A, with one exception: Equation 13 is replaced by:

$$\bar{r}_{jkl} = median\left(\frac{u^{th}_{ijkl}}{u^{m}_{ijkl}}\right)_{i=1,Neq} \qquad [16]$$

where $\bar{r}_{jkl}$ is the *median* ratio (in contrast to the *mean* ratio) of the residuals between the theoretical $\mathbf{u}^{th}$ and measured $\mathbf{u}^{m}$ displacements for the j^{th} site, k^{th} component and l^{th} phase. N_{eq} is the number of equations and is less than or equal to the number of events in the cluster, as before.

In the case of a normal distribution of residuals, the mean and median will be the same, and Scheme B will give the same results as Scheme A. However, if the distribution is skewed, the mean and median residuals will differ and the methods will give different results.

Scheme C – weighted mean correction

Schemes A and B are very similar, differing only in the definition of $\bar{r}_{jkl}$. This scheme differs from the previous two schemes because the residuals are computed from the differences between the observed and theoretical displacements (rather than the ratio of theoretical to observed displacement) and the weighting function is relatively simple (in contrast to the complex weighting function that consisted of an attenuation function and a smoothing function). As before, the scheme is described in a stepwise fashion.

1. Calculate the theoretical displacements $\mathbf{u}^{th}$ from Equation 10 after solving Equation 9 in a least-squares sense (as for steps 1 and 2 in Scheme A and B).

2. For the i^{th} event in the cluster, j^{th} site, k^{th} component and l^{th} phase, the residuals ε_{ijkl} between the theoretical and measured or observed displacements are calculated according to:

$$\varepsilon_{ijkl} = u^{obs}_{ijkl} - u^{th}_{ijkl} \qquad [17]$$

3. A weighting factor (ω_{ijkl}) is determined from the residuals of all the events in the cluster and is applied to the input data in the following way:

$$u^{new}_{ijkl} = \omega_{ijkl} \cdot u^{old}_{ijkl} \qquad [18]$$

where $u^{old}_{ijkl} = u^{obs}_{ijkl}$ for the first iteration and ω_{ijkl} is computed using:

$$\omega_{ijkl} = \frac{1}{1 + d^{2}_{ijkl}} \qquad [19]$$

In Equation 19, d_{ijkl} is the number of standard deviations the residual ε_{ijkl} is away from the mean residual $\bar{\varepsilon}_{jkl}$ (for event i, site j, component k and phase l) defined by:

$$d_{ijkl} = \frac{\varepsilon_{ijkl} - \bar{\varepsilon}_{jkl}}{s_{jkl}} \qquad [20]$$

where s_{jkl} is the unbiased standard deviation of the residuals. The mean residual $\bar{\varepsilon}_{jkl}$ and unbiased standard deviation s_{jkl} of the residuals are computed using Equations 21 and 22, respectively:

$$\bar{\varepsilon}_{jkl} = \frac{1}{N_{eq}} \sum_{i=1}^{N_{eq}} \varepsilon_{ijkl} \qquad [21]$$

$$s_{jkl} = \sqrt{\frac{1}{(N_{eq} - 1)} \sum_{i=1}^{N_{eq}} \left(\varepsilon_{ijkl} - \bar{\varepsilon}_{jkl}\right)^2} \qquad [22]$$

If $u_{ijkl}^{th} = u_{ijkl}^{obs}$ for all events in the cluster (i = 1 to N_{eq}) for a particular site (and component and phase), the standard deviation s_{jkl} will be zero, and ω_{ijkl} = 1. (When s_{jkl} = 0, Equation 20 is undefined and some exception handling in the computer code is necessary). Since ω_{ijkl} =1, no change will be made to the observed data in Equation 18 (as mentioned before, this will rarely be the case for real, recorded data).

If $u_{ijkl}^{th} \approx u_{ijkl}^{obs}$ for most of the events in the cluster, the standard deviation s_{jkl} will be small, and ω_{ijkl} will be close to 1 (such that $\omega_{ijkl} < 1$), and very little change will be made to the observed data.

If some of the data are noisy, and $u_{ijkl}^{th} \neq u_{ijkl}^{obs}$ for several events in the cluster, the standard deviation will be larger, and $\omega_{ijkl} << 1$. As a result, ω_{ijkl} will have a damping effect on the noisy data.

4. A new set of moment tensor components is then recomputed for each event using the corrected data:

$$\mathbf{m}_i^{new} = \mathbf{G}_i^{-1} \mathbf{u}_i^{new} \qquad [23]$$

5. As with the other schemes, this one can be applied iteratively by returning to step 2 and repeating the process. However, in contrast, the maximum number of iterations is not limited. Once again, the 'best' solution is identified on the basis of the minimum standard error normalised against the scalar moment (Equation 15).

This scheme shares a common characteristic with Scheme A – a sensitivity to outliers because the correction or weighting is dependent on the standard deviation of the normal distribution.

2.3 Stability tests: application of hybrid MTI to synthetic data

In any inversion procedure, it is necessary to demonstrate that the results are reliable and physically meaningful. Before applying the hybrid MTI methods to a case study situation, several stability tests were carried out to determine the limitations of the method and possible sources of error. This knowledge will enable the interpreter to distinguish between artefacts introduced by processing and meaningful output.

A number of stability tests using synthetic data were carried out to quantify the source resolving capabilities of the hybrid methods under various extreme conditions. The synthetic events were pure double-couple sources having identical fault-plane orientations, and differing only in rake. This similarity in the mechanisms was chosen because the waveforms of tightly grouped events recorded underground often show high degrees of similarity.

For each test, the results computed using the three hybrid methods were compared with one another and with those computed using the single event, absolute method and two relative methods (with and without a reference mechanism). In the noise-free situation, it was found that the relative method without reference mechanism showed the highest resolution of mechanisms, provided that the coverage of the focal sphere was not too sparse (> 3 stations). The hybrid method using a median correction was found to be the most robust of all the methods tested in the most extreme case of poor coverage (2 stations) of the focal sphere.

When increasing levels of pseudo-random noise were applied to the data, the absolute MTI method, the hybrid method using a median correction, and the hybrid method using a weighted mean correction all showed similar robustness and stability in extreme configurations concerning network coverage of the focal sphere and noise level. When increasing levels of systematic noise were added to the data, the hybrid methods using a median correction and weighted mean correction were found to exhibit similar robustness and stability in extreme configurations concerning network coverage of the focal sphere and systematic noise. In all situations investigated, these two hybrid methods outperformed the relative and absolute methods.

2.4 Case study: application of hybrid MTI to recorded data

In the thesis, two of the three hybrid MTI methods were applied to a cluster of events recorded at Oryx Gold Mine because both methods showed similar robustness and stability in the presence of random and systematic noise. However, for the sake of brevity, only the results computed using the hybrid method with a median correction are presented in this summary. The results are compared with those determined using absolute methods.

Seismic network and event cluster

The seismic network at Oryx Gold Mine is a PRISM system and consists of 7 triaxial geophones located at various depths on the mine's lease area. The network has a sensitivity of approximately M_L = -1 and a location accuracy of around 20 m. The event cluster considered in this study is positioned ahead of an advancing stope at a depth of approximately 2500 m (Figure 4b). The cluster was selected for closer study due to the noticeably tight spatial grouping, which becomes even more evident when the data set is filtered with respect to event magnitudes. The entire data set recorded between March 1999 and June 2000 consisted of 6495 events and is shown in Figure 4(a). The filtered data set (displaying events having local magnitudes > 0) consists of 78 events, and is displayed in Figure 4(b). Only the seismograms of the filtered data set were available for this study.

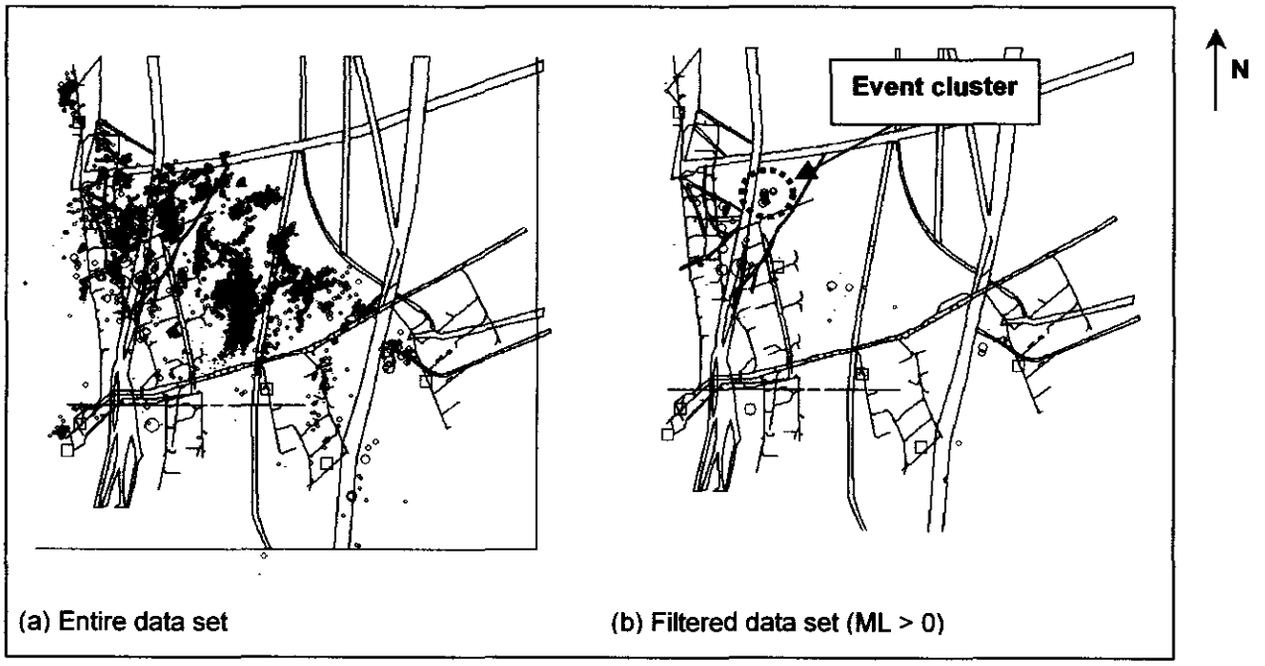

Figure 4: Plan view of events recorded at Oryx Gold mine (a) Entire data set: 6495 events recorded between March 1999 and May 2000 (b) Filtered data set: 78 events having local magnitudes M_L > 0 recorded during the same time period. Open squares represent the seven geophone sites, each consisting of three orthogonal geophones

Data description

The cluster selected for investigation consists of 10 of the 78 events, and the local magnitude M_L for these events ranges from 0 to 1.4 (Table 1), recorded over a time period of approximately 6 months.

Table 1: Event parameters

Event ID	Date	Time	M_L	X (m)	Y (m)	Z (m)	Error (m)
991014004	14/10/1999	08:04:39	0.4	3117570	26493	-2538	13.5
991118076	18/11/1999	16:50:11	0.5	3117572	26502	-2535	11.8
991123066	23/11/1999	17:04:10	0.2	3117549	26496	-2502	5.9
991123074	23/11/1999	17:43:53	1.4	3117571	26532	-2502	6.4
991127024	27/11/1999	13:35:28	0.9	3117571	26508	-2536	10.7
991206128	06/12/1999	17:11:46	1.4	3117563	26516	-2511	7.6
991213000	13/12/1999	04:24:36	0.4	3117573	26525	-2530	7.9
1000112007	12/01/2000	13:53:23	0.0	3117564	26520	-2528	9.4
1000328082	28/03/2000	18:56:44	0.5	3117527	26534	-2509	10.6
1000331112	31/03/2000	23:38:45	0.2	3117524	26525	-2509	15.8

Not only is the cluster of events tightly grouped in space, but also some of the waveforms of the events are very similar. This implies that the underlying source mechanisms are very similar. The waveform similarity is illustrated in Figure 5. The waveforms shown in the figure are the velocity traces recorded by a single geophone. The waveforms are plotted using the same time scale on the x-axis and no filters have been applied. Inspection of the traces reveals that some of the traces are almost indistinguishable from one another, especially the S-wave packages.

In many cases, the S-waves are not simple pulses but have an additional higher frequency component. However, this study assumes a simple impulsive source model and, for this reason, the moment tensor solutions will describe the average or dominant source mechanism.

Moment tensor inversion

The distances from the event cluster to the receivers range from ~350 m (site 5) to ~2000 m (site 3). The Brune source radius of the largest event is ~ 57 m (M_L = 1.4). Since the source radius of the largest event in this cluster is much less than the distance to the closest geophone site, the far-field approximation is satisfied.

The hybrid MTI method was applied to the event cluster where corrections were applied using medians of errors. Absolute moment tensors were used as starting values for the hybrid methods and were retained for comparative purposes. The inputs to both inversion methods consisted of the spectral plateaus of both P- and S-waves at frequencies below the corner frequency of the time-integrated displacement traces (Figure 6). The seismograms were not rotated into P, SV and SH phases and Equation 1 was applied to each phase with good signal to noise ratio, spectral fits and clear polarities.

Only phases with well-defined spectral inversions and polarities were used. The spectral fits presented in Figure 6 were obtained using the method described in Spottiswoode (1993).

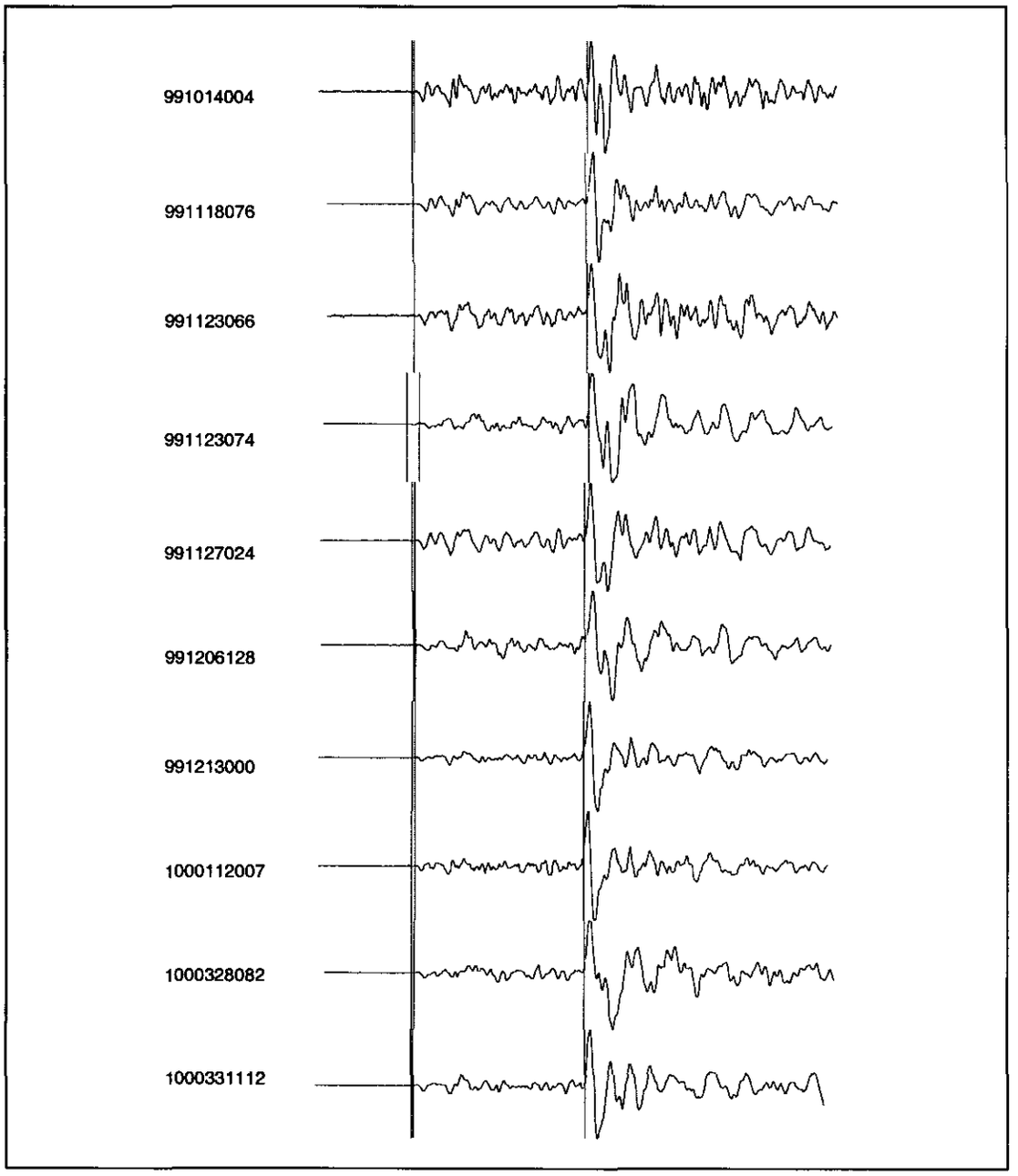

Figure 5: Velocity waveforms plotted using the same time axis as recorded by site 1, component 2. Note similarity of waveforms.

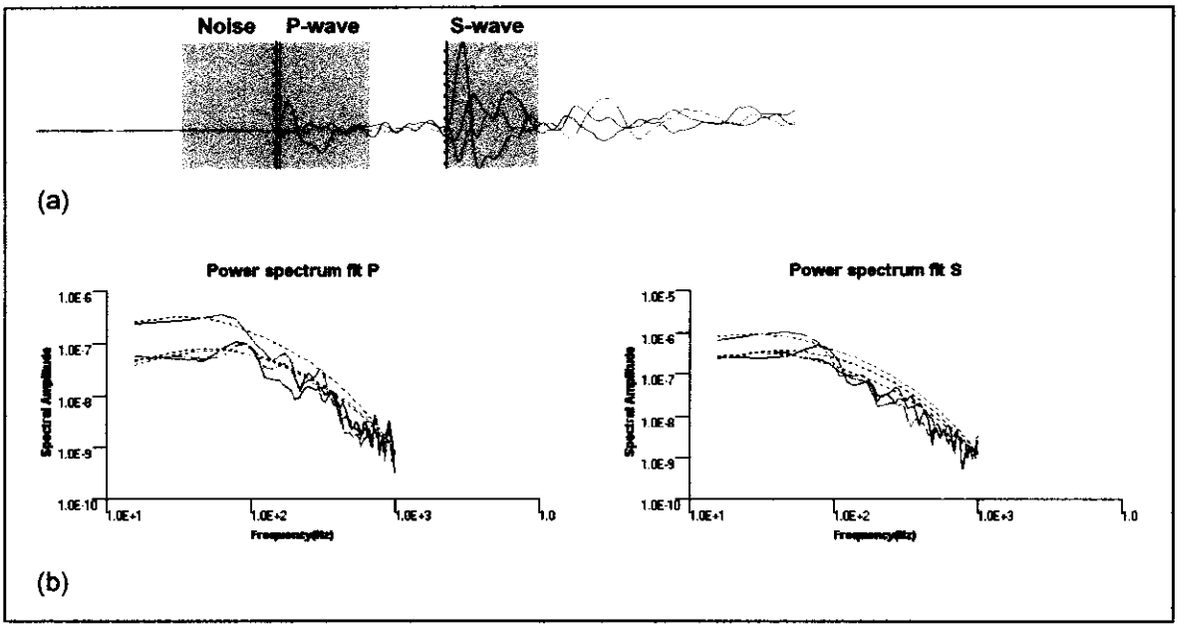

Figure 6: (a) Typical velocity seismograms. (b) Velocity spectra calculated from the raw traces (solid line), spectral fits (dotted lines) and noise spectra for the P -waves and S-waves for three geophones at one site. Cosine tapering was applied and spectra were smoothed with 3-point averaging.

First-motion polarities are not always clear due to several types of departure from the "ideal" data. Noise, head waves and P-wave coda waves prior to S-wave arrivals all complicate the choice of first motion. This is especially true if automatic processing is required. As the spectral plateaus are, in effect, derived from the largest "surge" in ground displacement, the direction of motion of this "surge" was sought. This was achieved by writing a synthetic seismogram based on the fitted spectrum of each phase and by matching this seismogram to the observed seismogram through cross-correlation. The direction of motion was then based on the presence of a single high (positive or negative) peak in the cross-correlation between these two functions. Absence of such a peak indicated that the direction was not well determined.

It is important to note that no outlier rejections were applied. The corrections were based purely on the distribution of the residuals.

To aid interpretation, the computed moment tensors are decomposed into components of source models using the formulation given by Knopoff & Randall (1970). The isotropic component, ISO%, is a measure of the volume change at the source and is calculated from the trace of the Euclidean normalised moment tensor M:

$$ISO\% = \frac{100\, tr(M)}{|tr(M)| + \sum_{i=1}^{3} |m_i^*|} \qquad [24]$$

where the m_i^* are the eigenvalues of the deviatoric moment tensor and are ordered according to magnitude and the trace is computed by summing the eigenvalues m_i of the

full tensor: $tr(M) = m_1 + m_2 + m_3$. The polarity of ISO% gives the direction of motion relative to the source with positive outwards e.g. –ISO% indicates an implosion.

The percentage contribution of the double-couple component to the full mechanism can be computed using:

$$DC\% = \frac{m_3^*(1-2F)}{|m_3^*(1-2F)| + |2m_3^* F|}(100 - \%ISO) \qquad [25]$$

where $F = -m_1^* / m_3^*$ and $m_i^* = m_i - \frac{1}{3}tr(M)$.

An additional quantity, the deviation ε of the seismic source from the model of pure double-couple, is calculated. This value is expressed as the ratio of the minimum to maximum deviatoric eigenvalue:

$$\varepsilon = \left| \frac{m_3^*}{m_1^*} \right| \qquad [26]$$

where the eigenvalues are ordered in the absolute sense and $\varepsilon = 0$ for a pure double-couple source, and $\varepsilon = 0.5$ for a pure CLVD (Compensated linear vector dipole) (Dziewonski *et al.*, 1981).

Results

One of the difficulties in moment tensor inversions is proving that the results provide an accurate reflection of reality. The only way this verification can be reliably undertaken is to obtain a detailed fracture mapping of the area of interest and compare the locations and orientations of the computed fault-plane solutions with those of the mapping. Even then, the conclusions often remain speculative. In the absence of such mapping, lesser techniques must be used. In this particular case study, the similarity of the waveforms plays an important role in assessing the integrity of the hybrid moment tensor solutions in the sense of whether or not they are any better than those determined using absolute methods. Since the input waveforms of the cluster show such close similarity, it is reasonable to expect the output moment tensors and their corresponding radiation patterns to exhibit similar likenesses.

The radiation patterns and fault-plane solutions of the cluster computed using the absolute MTI method are shown in Figure 7. The Cartesian moment tensors, source parameters and fault-plane solutions for the cluster are listed in Tables 2, 3 and 4. It is evident from the radiation patterns (Figure 7) and their corresponding fault-plane solutions that the results computed using the absolute MTI are more varied than would be expected from a source cluster having very similar waveforms. In Table 3, ISO% and DC% do not add up to 100% because ISO% is computed from the complete moment tensor whereas DC% is computed from the deviatoric part of the moment tensor.

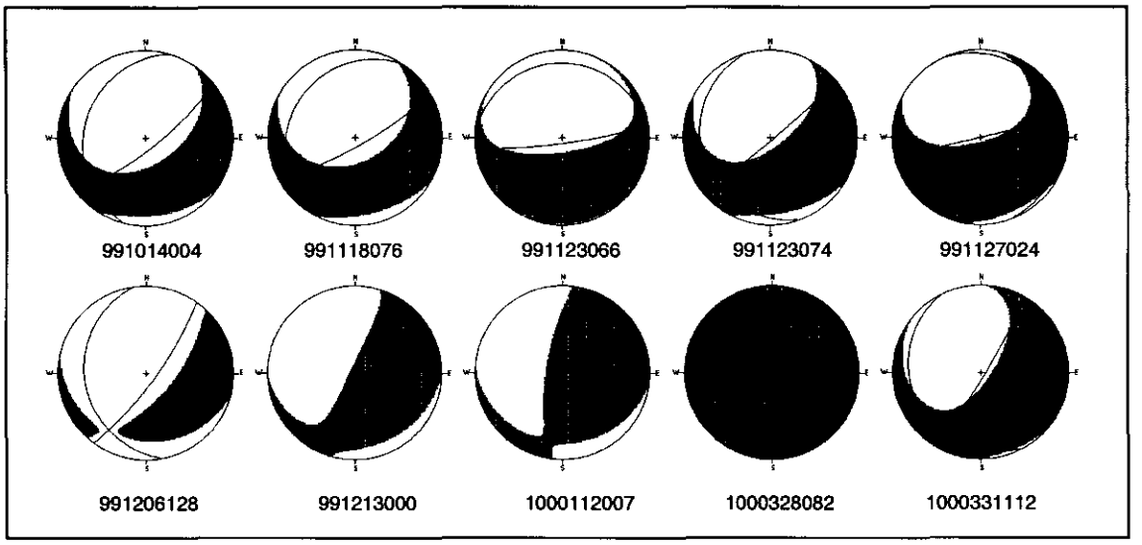

Figure 7: Radiation patterns and fault-plane solutions for the cluster computed with an absolute MTI.

Table 2: Cartesian moment tensor components for the Oryx cluster (Absolute MTI method)

Event ID	**Cartesian moment tensors (10^9 N.m) rotated into geographical (North, East, Down) system**					
	M_{11}	M_{12}	M_{13}	M_{22}	M_{23}	M_{33}
991014004	-3.00	1.25	-14.29	3.31	6.65	-20.07
991118076	-5.00	3.59	-23.75	5.76	9.22	-28.67
991123066	-3.46	1.53	-8.69	0.90	7.78	-13.61
991123074	-9.76	11.31	-321.47	20.43	47.74	-217.98
991127024	-12.65	9.48	-51.92	15.03	33.60	-28.45
991206128	-9.32	20.77	-114.95	25.90	32.66	-22.99
991213000	-2.49	4.36	-9.21	0.00	20.44	5.15
1000112007	-0.53	2.39	-0.47	0.46	10.94	8.91
1000328082	4.58	-1.72	-1.20	19.74	10.98	25.66
1000331112	-0.84	18.97	-75.95	32.71	105.03	-51.66

Table 3: Source parameters for the Oryx cluster (Absolute MTI method)

Event ID	**Deviation from DC (ε)**	**ISO%**	**DC%**
991014004	0.58	-20.0	12.4
991118076	0.66	-19.2	19.7
991123066	0.33	-25.1	34.2
991123074	0.43	-14.5	68.5
991127024	0.55	-10.5	65.7
991206128	0.28	-1.00	43.4
991213000	0.02	1.71	95.4
1000112007	0.45	18.9	67.8
1000328082	0.36	33.3	70.4
1000331112	0.19	0.8	62.7

Table 4: Fault-plane solutions for the Oryx cluster (Absolute MTI method)

Event ID	Fault-plane solution 1 (degrees)			Fault-plane solution 2 (degrees)		
	Strike	Dip	Rake	Strike	Dip	Rake
991014004	194.9	19.5	-125.3	51.8	74.2	-78.4
991118076	211.0	14.4	-118.9	60.7	77.5	-82.9
991123066	170.7	19.4	-133.4	35.8	76.1	-76.4
991123074	270.4	8.9	-82.0	82.3	81.2	-91.2
991127024	161.0	12.3	-158.5	50.0	85.5	-78.6
991206128	337.6	5.1	-8.9	76.5	89.2	-95.1
991213000	84.2	10.9	148.8	204.9	84.4	80.6
1000112007	57.7	17.3	136.3	190.0	78.2	77.3
1000328082	245.0	55.9	42.4	127.9	56.1	137.5
1000331112	152.0	12.6	-148.0	30.6	83.4	-79.3

The hybrid MTI method using a median correction gives radiation patterns and fault-plane solutions showing a high degree of similarity (Figure 8), indicating that these solutions are very probably more accurate reflections of reality than the absolute moment tensor solutions. The Cartesian moment tensor components, source parameters and fault-plane solutions for the cluster are listed in Tables 5, 6 and 7.

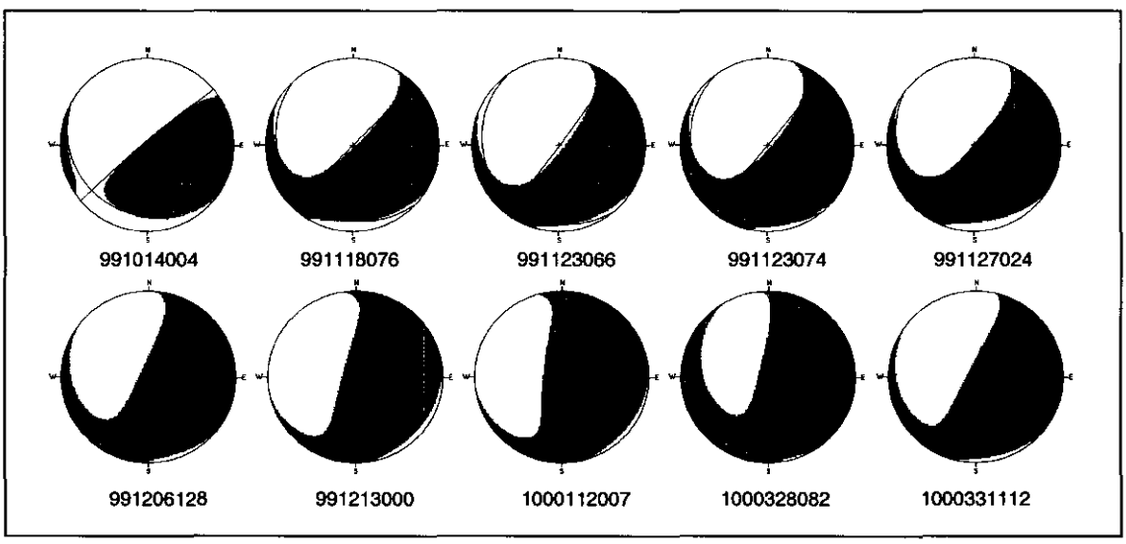

Figure 8: Radiation patterns and fault-plane solutions for the cluster computed with the hybrid MTI using a median correction.

There is a noticeable decrease in the isotropic components (compare ISO% of Tables 3 and 6) in this second set of results. There has been much discussion in the literature about the interpretation of non-double-couple components (i.e. the presence of isotropic components and deviations from the pure double-couple model). Most of the debate is centred on whether the non-double-couple components are intrinsic to the source rupture process or artefacts of processing (due to inappropriate modelling of the ray-path, the presence of noise, invalid source models, etc.). This study shows that the percentage of isotropic component can be decreased significantly by application of the hybrid MTI method with median correction.

The 'sharpening up' of the solutions described earlier is an encouraging phenomenon, and is a strong indicator of the hybrid method's potential for use as a standard processing tool for mine seismicity.

Table 5: Cartesian moment tensor components for the Oryx cluster (Hybrid MTI)

Event ID	Cartesian moment tensors (10^9 N.m) rotated into geographical (North, East, Down) system					
	M_{11}	M_{12}	M_{13}	M_{22}	M_{23}	M_{33}
991014004	-2.84	0.05	-8.21	1.31	7.39	2.28
991118076	-3.77	2.09	-15.22	3.78	14.32	-1.87
991123066	-1.09	1.38	-7.52	1.58	9.37	-2.55
991123074	-14.72	21.83	-138.73	41.87	153.77	-29.32
991127024	-7.91	7.70	-37.38	11.31	42.51	-0.37
991206128	-2.07	13.75	-40.22	23.58	98.23	46.23
991213000	1.01	3.04	-6.02	-1.05	26.32	17.97
1000112007	0.95	1.39	-0.56	-0.21	12.40	11.49
1000328082	0.41	2.45	-2.11	7.23	12.81	6.07
1000331112	-5.26	10.33	-50.49	19.93	109.61	51.84

Table 6: Source parameters for the Oryx cluster (Hybrid MTI)

Event ID	Deviation from DC (ε)	ISO%	DC%
991014004	0.03	-0.21	93.5
991118076	0.19	-3.5	62.3
991123066	0.23	-5.0	76.1
991123074	0.11	1.8	77.5
991127024	0.09	2.4	82.31
991206128	0.33	18.6	71.7
991213000	0.32	16.9	71.9
1000112007	0.41	22.0	18.2
1000328082	0.27	26.1	46.8
1000331112	0.31	16.2	72.1

Table 7: Fault-plane solutions for the Oryx cluster (Hybrid MTI)

Event ID	Fault-plane solution 1			Fault-plane solution 2		
	Strike	Dip	Rake	Strike	Dip	Rake
991014004	116.9	11.4	156.7	229.8	85.5	79.6
991118076	134.6	10.3	179.8	224.7	90.0	79.7
991123066	142.4	8.3	-164.0	36.5	87.7	-82.0
991123074	142.0	9.0	-167.7	39.8	88.1	-81.2
991127024	125.2	10.9	175.6	219.6	89.2	79.1
991206128	88.0	11.2	152.9	204.6	84.9	80.0
991213000	38.2	11.3	113.1	194.6	79.6	85.5
1000112007	30.0	14.1	113.4	185.9	77.1	84.3
1000328082	101.6	16.5	176.7	194.8	89.1	73.5
1000331112	82.2	9.4	145.0	206.8	84.6	82.3

3. Practical implications of this study

As already alluded to in the abstract, insight into the source mechanisms of mine tremors contributes to understanding the various modes of failure observed around underground excavations in the mining environment. The planes of failure may be caused by stresses induced by mining or be of geological origin. Knowledge of the geometry of these failure planes is critical in the mine-planning process so that tunnels are not planned in unfavourable orientations with respect to major geological structures.

The MTI methods currently applied on the mines are not always reliable and are sensitive to many different sources of error. The hybrid MTI methods developed by the author aim to increase the accuracy of the moment tensor solutions by reducing the effect of noisy data and correcting for geophone site effects. In the case study, the solutions computed using the hybrid method are more focussed than those calculated using the absolute method and show fine distinctions amongst the events not evident from the absolute solutions. The improved moment tensor solutions will then provide more opportunities for interpreting mine seismicity in terms of driving stresses and geological features, ultimately leading to improved safety underground.

A computer program, the 'MTI toolbox', was written by the author to perform the hybrid MTI techniques. This program is compatible with AURA[2] and enables moment tensors to be computed quickly and easily. Since the analysis in the case study was based on these automatic procedures, the hybrid MTI methods have the potential of being applied routinely in processing mine seismic data.

The hybrid MTI methods are being used in the following environments:

- The research environment. The hybrid MTI methods were applied extensively to seismograms recorded by an ISS[3] seismic system and converted into PRISM[4] format for processing in AURA during the course of a SIMRAC[5] project that investigated the mechanisms of failure near a dip-stabilizing pillar (GAP604). The moment tensor analysis was useful in determining failure trends and assessing the regional stress state of the study area.

- The hybrid MTI methods are currently being applied to seismograms recorded by a PRISM system installed at Impala Platinum Mine near Rustenburg, South Africa. The hybrid MTI software performs the calculations on a data file generated by AURA.

- The hybrid methods are currently being tested by Snowden Mining Industry Consultants on waveform data recorded in Western Australia by the GMM[6].

---

2 AURA is the seismological processing and analysis software written by CSIR Miningtek that reads data recorded by both PRISM and GMM.

3 Integrated Seismic System developed by ISS International Ltd.

4 PRISM is a digitally networked real-time seismic monitoring system for mine-wide application developed by CSIR Miningtek, M&M Systems and Goldfields (then GenMin).

5 Safety in Mines Research Advisory Committee.

6 GMM, the Ground Motion Monitor, is a low cost portable seismic recording device designed to monitor relatively small volumes of rock.

- Application of the hybrid MTI method is not limited to the mining environment but may also be useful in the laboratory. In rock mechanics, studies of acoustic emission data has often been used to monitor damage and failure in brittle materials. MTI methods applied to acoustic emission data are subject to similar sources of error as seismic data recorded on a macro-scale in the mining environment. Since these micro-events also occur in clusters and the common ray-path approximation holds, the hybrid MTI methods could be used to enhance the moment tensor solutions of acoustic emission data, providing greater insight into the brittle fracture process. The hybrid MTI methods are to be applied to acoustic emission data in a collaborative project entitled 'Non-destructive evaluation of concrete structures using acoustic and electro-magnetic methods' funded by the German National Science Foundation (FOR 384).

References

Aki, K. & Richards, P.G. (1980). *Quantitative Seismology,* Freeman, San Francisco.

Barker, J.S. & Langston, C.A. (1982). Moment tensor inversion of complex earthquakes, *Geophys. J. R. Astr. Soc.* **46**, pp341–371.

Brawn, D.R. (1989). *A maximum entropy approach to underconstraint and inconsistency in the seismic source inverse problem; Finding and interpreting seismic source moments*, Ph.D. Thesis, University of the Witwatersrand, Johannesburg.

Dahm, T. (1996). Relative moment tensor inversion based on ray theory: theory and results, *Geophys. J. Int.* **124**, pp245–257.

Dziewonski, A.M., Chou T.A. & Woodhouse, J.H. (1981). Determination of earthquake source parameters from waveform data for studies of local and regional seismicity, *J. Geophys. Res.* **86**, pp2825 – 2852.

Gilbert, F. & Dziewonski, A.M. (1975). An application of normal mode theory to the retrieval of structural parameters and source mechanisms from seismic spectra. *Phil. Trans. R. Soc. Lond. A.* **278**, pp187-269.

Knopoff, L. & Randall, M.J. (1970). The compensated linear vector dipole: a possible mechanism for deep earthquakes, *J. Geophys. Res.* **75**, pp4957–4963.

Oncescu, M.C. (1986). Relative seismic moment tensor determination for Vrancea intermediate depth earthquakes, *Pure Appl. Geophys.* **124**, pp931–940

Patton, H. (1980). Reference point equalisation method for determining the source and path effects of surface waves, *J. Geophys. Res.* **85**, pp821–848.

Šílený, J., Panza, G.F. & Campus, P. (1992). Waveform inversion for point source moment tensor retrieval with variable hypocentral depth and structural model. *Geophys. J. Int.* **109**, pp259–274.

Spottiswoode, S.M. (1984). Source mechanisms of mine tremors at Blyvooruitzicht gold mine. In: N.C. Gay & E.H. Wainwright (Eds.) *Rockbursts and Seismicity in Mines*, Balkema, pp29–37.

Spottiswoode, S.M. (1993). Seismic attenuation in deep-level mines, In: R.P Young (Ed.) *Rockbursts and Seismicity in Mines*, Balkema. pp409-414.

Strelitz, R.A. (1978). Moment tensor inversions and source models, *Geophys. J.* **52**, pp359–364.

Strelitz, R.A. (1980). The fate of the downgoing slab: A study of the moment tensors from body waves of complex deep-focus earthquakes, *Phys. Earth. Planet. Int.* **21**, pp83–96.

Udias, A. & Baumann, D. (1969). A computer program for focal mechanism determination combining P and S wave data. *Bull. Seism. Soc. Am.* **59**, pp503–519.

ecipients of the Rocha Medal

1982	A.P. Cunha	PORTUGAL	Mathematical Modelling of Rock Tunnels
1983	S. Bandis	GREECE	Experimental Studies of Scale Effects on Shear Strength and Deformation of Rock Joints
1984	B. Amadei	FRANCE	The Influence of Rock Anisotropy on Measurement of Stresses in Situ
1985	P.M. Dight	AUSTRALIA	Improvements to the Stability of Rock Walls in Open Pit Mines
1986	W. Purrer	AUSTRIA	Calculation Model for the Behaviour of a Deep-Lying Seam Roadway in a Solid (but cut by Bedding Planes) Surrounding Rock Mass, taking into Consideration the Failure Mechanisms of the Soft Layer Determined In-Situ on Models
1987	D. Elsworth	UNITED KINGDOM	Laminar and Turbulent Flow in Rock Fissures and Fissure Networks
1988	S. Gentier	FRANCE	Morphology and Hydromechanical Beheviour of a Natural Fracture in a Granite, under Normal Stress – Experimental and Theoretical Study
1989	B. Fröhlich	GERMANY	Anisotropic Swelling Behaviour of Diagenetically Consolidated Claystones
1990	R.K. Brummer	SOUTH AFRICA	Fracturing and Deformation at the Edges of Tabular Gold Mining Excavations and the Development of a Numerical Model describing such Phenomena
1991	T.H. Kleine	AUSTRALIA	A Mathematical Model of the Rock Breakage by Blasting
1992	A. Ghosh	INDIA	Fractal and Numerical Models of Explosive Rock Fragmentation
1993	O. Reyes W.	PHILIPPINES	Experimental Study and Analytical Modelling of Compressive Fracture in Brittle Materials
1994	S. Akutagawa	JAPAN	A Back Analysis Program System for Geomechanics Application
1995	C. Derek Martin	CANADA	The Strength of Massive Lac du Bonnet Granite around Underground Openings
1996	M. P. Board	USA	Numerical Examination of Mining-Induced Seismicity
1997	M. Brudy	GERMANY	Determination of In-Situ Stress Magnitude and Orientation of 9 km Depth at the KTB Site
1998	F. Mac Gregor	AUSTRALIA	The Rippability of Rock
1999	A. Daehnke	SOUTH AFRICA	Stress Wave and Fracture Propagation in Rock
2000	P. Cosenza	FRANCE	Coupled Effects between Mechanical Behaviour and Mass Transfer Phenomena in Rock Salt
2001	D. F. Malan	SOUTH AFRICA	An Investigation into the Identification and Modelling of Time-Dependent Behaviour of Deep Level Excavations in Hard Rock
2002	M.S.Diederichs	CANADA	Instability of Hard Rockmasses: the Role of Tensile Damage and Relaxation
2003	L. M. Andersen	SOUTH AFRICA	A Relative Moment Tensor Inversion Technique applied to Seismicity Induced by Mining
2004	G. Grasselli	ITALY	Shear Strength of Rock Joints based on the Quantified Surface Description
2005	M. Hildyard	UNITED KINGDOM	Wave Interaction with Underground Openings in Fractured Rock
2006	D. Ask	SWEDEN	New Developments of the Integrated Stress Determination Method and Application to the ÄSPÖ Hard Rock Laboratory, Sweden